Performance of Different Soil Model Configurations in Simulating Ground Surface Temperature and Surface Fluxes

Tatiana G. Smirnova,* John M. Brown, and Stanley G. Benjamin

NOAA/ERL Forecast System Laboratory, Boulder, Colorado

ABSTRACT

This study compares three modifications to the one-dimensional planetary boundary layer scheme that is implemented in the σ–θ hybrid-b version of the Mesoscale Analysis and Prediction System (MAPS) and the Rapid Update Cycle (RUC). All three modifications are based on the incorporation of a simple soil model into the basic version to more accurately calculate the moisture and heat fluxes across the ground surface. The presented schemes are of increasing sophistication: the first model combines the soil model with heat and moisture budget equations for the ground surface and uses an explicit numerical scheme to compute the surface fluxes; the second model uses a more energy-conservative implicit solution for the latent and sensible surface fluxes and heat and moisture soil fluxes; the third model further incorporates a simple parameterization of the evapotranspiration process.

The comparison includes the effect of different schemes on diurnal changes of surface temperature and soil heat flux. The schemes are tested for two case studies; a dry case from the O'Neill, Nebraska, Great Plains Turbulence Field Program and a moist case from the First ISLSCP (International Satellite Land Surface Climatology Project) Field Experiment. Tests are performed to evaluate sensitivity to soil parameters related to thermal diffusivity and to vertical resolution of the soil scheme. Overall, the comparison supports the idea that implementation of a multilevel soil model is competitive with and can even improve the ground surface temperature forecast over that produced by the present MAPS implementation of the force restore method. The case study demonstrates that incorporation of a primitive evapotranspiration model can give positive results.

1. Introduction

Heat and moisture exchanges between the ground surface and the atmosphere are frequently dominant driving mechanisms for mesoscale circulations. These surface processes are included in weather forecast model physics by specifying different lower boundary conditions, depending on surface characteristics. Over land, where there are significant diurnal changes of temperature and moisture near the interface with the atmosphere, heat and moisture balance equations are usually used.

In particular, the prediction of the ground surface temperature and moisture content is critical to obtaining successful forecasts of heat and moisture exchange between ground and atmosphere. Two general approaches to predicting these variables have been used in past studies. The first approach does not consider heat and moisture exchange processes within the soil and uses

various empirical formulas for the calculation of soil flux near the ground surface. Many methods belonging to the first approach have been developed (Arakawa 1972; Manabe et al. 1974; Pielke 1974; Blackadar 1976; Deardorff 1978; Jacobsen and Heise 1982) and, because of their simplicity, are widely used in operational forecast models. However, for a variety of meteorological problems, this empirical approach to determining the ground surface temperature and soil moisture is not satisfactory. More accurate and reliable calculation of surface soil fluxes requires a detailed knowledge of soil temperature and soil moisture stratification (Chen et al. 1996). For this reason, the second approach is to use a multilayer soil model to calculate soil fluxes on the basis of time-dependent solutions for temperature and moisture in soil. It has the potential for improved accuracy through the simulation of heat and moisture exchange processes both at the ground surface and within the soil. This will, for instance, increase the sensitivity of the model forecasts to short-period occurrences of excessive or deficient precipitation, an important consideration for data assimilation systems intended for rapid updating on fine horizontal meshes. Of course, the second approach also has some disadvantages: the need for additional initial data for soil-related variables and for more computational resources. Therefore, its use has

---

*Additional affiliation: Cooperative Institute for Research in Environmental Sciences, Boulder, Colorado.

Corresponding author address: Dr. Tatiana G. Smirnova, NOAA/ERL/FSL, R/E/FS1, 325 Broadway, Boulder, CO 80303.
E-mail: smirnova@fsl.noaa.gov

usually been restricted to research models (e.g., Mahrer and Pielke 1977; McCumber and Pielke 1981; Sievers et al. 1982; Kiselnikova et al. 1984; Tremback and Kessler 1985; Pressman 1988) or in studies of soil hydrology and micrometeorology (e.g., de Vries 1958; Halstead et al. 1957). Nevertheless, recent progress in development of techniques for soil-moisture content initialization, and the construction of soil-type and soil characteristics and vegetation archives with high spatial resolution (e.g., Dickinson et al. 1986; Smith et al. 1994; Matthews 1984a,b; Zobler 1988), make it possible to incorporate soil models into operational mesoscale forecast models.

Recently, increased attention has been given to the parameterization of evapotranspiration through complex vegetation canopies for numerical prediction models. Biosphere models of various degree of complexity have been developed by Deardorff (1978), Garrett (1982), Anthes (1984), Dickinson (1984), Sellers et al. (1986), Wilson et al. (1987), Wetzel and Chang (1988) and Avissar and Pielke (1989) for use in general circulation and mesoscale models. Most of these models need the input of many vegetation parameters and have relatively high computational costs, not to mention the problem of initialization. A robust and computationally efficient evapotranspiration model was developed by Pan and Mahrt (1987). They implemented a very simple way to include the effect of vegetation through modifying the formulas that describe the fluxes of heat and water from the underlying soil. This model is widely used for experiments in local weather forecasting, air pollution, soil chemistry, and soil hydrology, and its concept is used in the present study for treating the evapotranspiration process.

This paper demonstrates that the second approach, using an unsophisticated soil–vegetation model for the forecast of heat and moisture exchange between the ground and atmosphere, can compete with the simpler empirical approach and even improve its results. The context of this demonstration is the isentropic–sigma hybrid model used in the Mesoscale Analysis and Prediction System (MAPS, Bleck and Benjamin 1993; Pan et al. 1994; Benjamin et al. 1991; Benjamin et al. 1996; Benjamin et al. 1997). The empirical method tested here, later identified as CONTROL, is used in the version of MAPS currently (early 1997) operational at the National Centers for Environmental Prediction (NCEP), the Rapid Update Cycle (RUC), but with climatological non-varying soil moisture in the RUC. In this paper, three configurations of a soil model are incorporated into a one-dimensional version of MAPS and their ground surface temperature forecasts are compared.

2. Soil model

A multilevel soil model traditionally consists of two main equations for heat and moisture transfer within soil. Heat conduction can be evaluated from the one-dimensional diffusion equation offered by de Vries (1952)

$$\frac{\partial T}{\partial t} = \frac{\partial}{\partial z}\left(\frac{\nu}{\rho_s c_s}\frac{\partial T}{\partial z}\right), \tag{1}$$

where ν, c_s, and ρ_s, are the thermal conductivity, specific heat capacity, and soil density, respectively. The expression $\nu/\rho_s c_s = k_s$ is called the thermal diffusivity. The quantity ν indicates the rate of heat transfer, and k_s determines the penetration into the soil of the diurnal temperature cycle. (A detailed list of symbols is given in appendix A and definitions of certain frequently used terms are included in appendix B.) Thermal conductivity is very sensitive to many factors, such as the size of soil particles, porosity, and amount of water in the soil. Based on the empirical data of Al Nakshabandi and Kohnke (1965), ν can be expressed in units of J (m s K)$^{-1}$ as (McCumber 1980)

$$\nu = \begin{cases} 418.46 \exp[-(P_f + 2.7)], & P_f \leq 5.1 \\ 0.172 & P_f > 5.1, \end{cases} \tag{2}$$

where $P_f = \log_{10}[\Psi_s(\eta_s/\eta)^b]$, Ψ_s is the moisture potential for saturated soil representing the potential energy needed to extract water against capillary and adhesive forces in the soil, η_s is the saturation moisture content (porosity), and η is the volumetric moisture content. Values of Ψ_s, η_s, and exponent b are specified as functions of eleven USDA (United States Department of Agriculture) textural classes of soil plus peat, as presented by Clapp and Hornberger (1978). The volumetric heat capacity of soil is calculated according to the weighted contribution of the dry soil and the liquid water that is present (McCumber 1980)

$$\rho_s c_s = (1 - \eta_s)\rho_i c_i + \eta\rho_w c_w, \tag{3}$$

where $\rho_i c_i$ is the volumetric heat capacity of the dry soil type i, and $\rho_w c_w$ is the water volumetric heat capacity. The heat capacity of air is neglected since its contribution is much smaller than those of the other two terms.

For computation of fluxes to and from the atmosphere, the vertical movement of groundwater is more important than horizontal movement. Therefore, a vertical one-dimensional equation of diffusive and gravitational motions for soil moisture transfer is usually used in soil models. It was mathematically represented by Richards (1931) and implemented into the first fundamental model of transport processes in the soil by Philip and de Vries (1957):

$$\frac{\partial \eta}{\partial t} = \frac{\partial}{\partial z}\left(D_\eta \frac{\partial \eta}{\partial z}\right) + \frac{\partial K_\eta}{\partial z}, \tag{4}$$

where D_η and K_η are diffusional and hydraulic conductivity, respectively. The conductivities can be expressed in terms of the volumetric moisture content using the empirical relations reported in Clapp and Hornberger (1978),

$$D_\eta = -\frac{bK_{\eta_s}\Psi_s}{\eta}\left(\frac{\eta}{\eta_s}\right)^{b+3}, \qquad (5)$$

$$K_\eta = K_{\eta_s}\left(\frac{\eta}{\eta_s}\right)^{2b+3}, \qquad (6)$$

where K_{η_s} is the saturated soil value of hydraulic conductivity. The magnitudes of K_{η_s}, Ψ_s, η_s, and b are functions of the soil textural class (Clapp and Hornberger 1978).

3. Surface balance equations

In representing the land surface as the lower boundary condition of an atmospheric model, it is convenient to consider bare soil separately from vegetated ground because the interaction of bare soil with the atmosphere is simpler. In our formulation, the greater complexity introduced by vegetation directly affects the latent heat flux through incorporation of evaporation of free water from the canopy as well as through evapotranspiration. In addition, rainwater may be intercepted by the canopy without reaching the ground.

a. Bare soil

Many mesoscale models (e.g., Physick 1976; Estoque and Gross 1981; Mahrer and Pielke 1977) use a heat budget technique in which the ground surface has no thickness and, therefore, no heat storage. In this case, all fluxes at the ground surface are in balance. Another technique that regards a thin layer spanning the ground surface and including both the soil and the atmosphere with corresponding heat capacities and densities (e.g., Blackadar 1976; Deardorff 1978; Wetzel 1978; Tremback and Kessler 1985; Sellers et al. 1986) is used for the purpose of this study. The heat storage of this layer is determined by the contributions of both atmospheric and soil fluxes.

The heat budget equation for the interface-spanning layer with average temperature T_g is written as

$$\rho c \frac{\partial T_g}{\partial t} = \frac{\partial}{\partial z}(R_n - H - L_v E + G), \qquad (7)$$

where R_n is net radiation, H is sensible heat flux, $L_v E$ is latent heat flux, and G is soil heat flux, $G = \nu \partial T/\partial z$. (Radiation fluxes are defined positive toward the surface, other fluxes positive away from the surface.) The integration in the area from the middle of the first layer in the soil up to the middle of the first atmospheric layer (Fig. 1) yields

$$(\rho_a c_p \Delta z_a + \rho_s c_s \Delta z_s)\frac{\partial T_g}{\partial t}$$
$$= (R_n - H - L_v E)|_{\Delta z_a} - G|_{-\Delta z_s}. \qquad (8)$$

The evaporation rate is calculated over the bare soil as
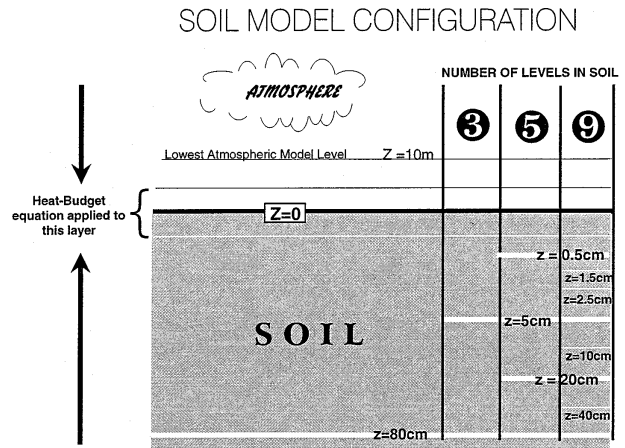
SOIL MODEL CONFIGURATION

FIG. 1. Soil model configuration, including depiction of the region spanning the surface used for the finite-difference solution of the heat and moisture budget equations. Three options for three-, five-, and nine-level schemes are shown.

$$E = E_{\text{dir}} = -\rho_a K_q \frac{\partial q_v}{\partial z}\bigg|_{\Delta z_a}, \qquad (9)$$

where K_q is the turbulent exchange coefficient for moisture determined using the three-layer aerodynamic scheme introduced by Pan et al. (1994), and q_v is the atmospheric water vapor mixing ratio.

The prediction of the soil moisture near the ground surface, important for surface processes, requires formulation of a moisture balance equation, which is written

$$\rho_w \frac{\partial \eta_g}{\partial t} = \frac{\partial}{\partial z}(W_s + I - E_1), \qquad (10)$$

where η_g is the average volumetric water content in the thin, near ground surface soil layer, I is the infiltration flux (which is positive toward the surface and equals precipitation minus runoff, where runoff is precipitation that cannot infiltrate because of the soil saturation), E_1 is the flux of total moisture content in the atmosphere, and W_s is soil moisture flux

$$W_s = \rho_w \left(D_\eta \frac{\partial \eta}{\partial z} + K_\eta\right), \qquad (11)$$

where D_η and K_η are determined by (5) and (6).

The flux of total moisture content between the ground surface and the first model level in the atmospheric domain can be written as

$$E_1 = -\rho_a K_q \frac{\partial q_a}{\partial z}\bigg|_{\Delta z_a}, \qquad (12)$$

where q_a is the total water content mixing ratio.

Equation (10) is integrated over the same area as for the heat budget equation (Fig. 1), giving

$$\rho_w \Delta z_s \frac{\partial \eta_g}{\partial t} = -W_s|_{-\Delta z_s} + (I - E_1)|_{\Delta z_a}. \qquad (13)$$

To close the system of Eqs. (10)–(12), (5), and (6) for moisture, a boundary condition must be provided near the earth's surface (Deardorff 1978)

$$q_a - q_g = M(q_a - q_{g_s}), \quad (14)$$

where M is the soil moisture availability, equal to the ratio of the available soil moisture content near the ground surface to the available moisture content at field capacity,

$$M = \frac{\eta_g - \eta_r}{\eta_{ref} - \eta_r}. \quad (15)$$

b. Vegetated surfaces

Vegetation cover is usually present, and it significantly influences the infiltration and evaporation processes. The transfer of moisture from the soil to the air mainly takes place through leaf transpiration. During the daytime in dry areas, vegetation can reduce evaporation and retain some soil moisture as the leaf stomata close if the soil moisture drops below a critical value (wilting point, see appendix B). In the case of light rainfall over forested areas, much of the rainwater can be intercepted by the leaves and reevaporated directly without ever reaching the ground. Further, the vegetation cover affects the absorption of solar radiation and exchange of sensible heat. Therefore, the influence of vegetation cover on the components of the heat and moisture balance equations at the surface is important.

More complicated treatments of surface processes in the presence of vegetation may be used for solving problems of soil hydrology and plant water budgets, but for operational weather forecasts of short range (such as those from the Rapid Update Cycle), simple models are presumably sufficient. In the present study a relatively simple approach will be used (Pan and Mahrt 1987), where evaporation from vegetation may occur as direct evaporation of liquid water from the canopy, E_c, as well as by transpiration, E_t. Direct evaporation from the canopy is expressed by

$$E_c = E_p \left(\frac{C^*}{S'} \right)^n. \quad (16)$$

Here we have chosen to specify the potential evaporation as $E_p = \rho_a K_q (q_{g_s} - q_a)/z_a$, S' is the saturation water content for a canopy surface, and n is a nondimensional parameter. The canopy water content ($C^* \leq S'$) is determined by

$$\rho_w \frac{dC^*}{dt} = P - E_c, \quad (17)$$

where P is the precipitation flux.

The transpiration flux is written as

$$E_t = \frac{E_p k_v \sum_{i=1}^{N} [\Delta z_i g(\eta_i)][1 - (C^*/S')^n]}{\sum_{i=1}^{N} [\Delta z_i]}, \quad (18)$$

where N is the number of levels within the root zone, k_v is a nondimensional plant resistance factor, and $g(\eta_i)$ is the transpiration rate function, defined as

$$g(\eta_i) = \begin{cases} 1, & \eta_i > \eta_{ref} \\ \dfrac{\eta_i - \eta_{wilt}}{\eta_{ref} - \eta_{wilt}}, & \eta_{ref} \geq \eta_i > \eta_{wilt} \\ 0, & \eta_{wilt} \geq \eta_i. \end{cases} \quad (19)$$

The parameter η_{ref} is the value of soil moisture below which the transpiration begins to decrease. When soil moisture decreases to the plant wilting factor (η_{wilt}), the transpiration stops (Mahrt and Pan 1984). Both parameters are functions of the soil textural classes listed by McCumber (1980). This simple formulation for E_t assumes both a constant rooting depth and uniform root distribution in the vertical.

For surfaces covered by vegetation, total evaporation consists of three components: direct evaporation from the bare soil, transpiration, and canopy evaporation, taken with corresponding weights

$$E = E_{dir}(1 - \sigma_f) + (E_c + E_t)\sigma_f, \quad (20)$$

where σ_f is a nondimensional plant shading factor, which varies between 0 and 1. It should be noticed that total evaporation is constrained to never exceed the potential evaporation and that it may be incorporated into the integrated form of heat balance equation [Eq. (8)] as

$$(\rho_a c_p \Delta z_a + \rho_s c_s \Delta z_s)\frac{\partial T_g}{\partial t}$$
$$= \{R_n - H - L_v[E_{dir}(1 - \sigma_f) + E_c\sigma_f$$
$$+ E_t\sigma_f]\}|_{\Delta z_a} - G|_{-\Delta z_s}. \quad (21)$$

The moisture balance equation for vegetated surfaces can be written as

$$\rho_w \Delta z_s \frac{\partial \eta_g}{\partial t}$$
$$= -W_s|_{-\Delta z_s} + \{(1 - \sigma_f)I + \sigma_f D$$
$$- E_1(1 - \sigma_f) - E_t\sigma_f\}|_{\Delta z_a}, \quad (22)$$

where

$$D = \begin{cases} P - E_c, & C^* \geq S' \\ 0, & C^* < S' \end{cases}$$

is excess water dripping from the vegetation canopy onto the soil when the canopy is saturated.

TABLE 1. Models used for calculating ground temperature and surface fluxes.

Model	Description
CONTROL	No computation of heat and moisture transfer inside soil. Force–restore treatment of ground soil temperature and moisture.
SOIL	Finite-difference solution of heat and moisture transfer equations within soil. Heat and moisture balance equations on the surface. Explicit treatment of atmospheric surface fluxes.
SOIL IMPLICIT	As in SOIL, but implicit treatment of atmospheric surface fluxes.
PLANT	As in SOIL IMPLICIT plus primitive plant canopy model.

4. Finite-differencing technique

In the present study, numerical experiments were conducted using four models (Table 1). The described equations for soil and canopy models, together with heat and moisture budget equations, were incorporated into a one-dimensional version of the MAPS atmospheric model. The original version, without soil or canopy model, is referred to hereafter as CONTROL (Pan et al.

1994). Following Deardorff [1978, his Eq. (12)], the soil moisture in CONTROL is taken into consideration through the force restore treatment. The particular parameterization of the soil heat flux used in CONTROL was taken from the NCAR–Penn State mesoscale model (MM4: Anthes et al. 1987; MM5: Grell et al. 1994; Zhang and Anthes 1982):

$$G = K_m C_g (T_g - T_m), \tag{23}$$

where K_m is the heat-transfer coefficient expressed through the angular velocity of the earth, Ω ($K_m = 1.18\Omega$); $C_g = 0.95(vc_s\rho_s/2\Omega)^{1/2}$ is the thermal capacity of the slab per unit area; and T_m is the temperature of the substrate, specified in section 5b.

In the first modification, referred to as SOIL, the soil model described in section 2 was incorporated into the basic model together with the moisture-budget equation for the ground surface. The soil model has nine levels: the first level is on the ground surface and the rest are at the depths 0.5, 1.5, 2.5, 5.0, 10.0, 20.0, 40.0, and 80.0 cm. The fully implicit Crank–Nicholson scheme was used for the heat diffusion equation in soil. It is accurate to second order and stable for all time intervals. The soil model also employs a fully implicit scheme for the moisture transfer equation with the linearization of hydraulic conductivity from (6) as $K'_\eta(\eta^n) = (K_{\eta_s}/\eta_s)(\eta^n/\eta_s)^{2b+2}$. In finite-difference form, (1) and (4) are written as

$$\frac{T_i^{n+1} - T_i^n}{\Delta t} = \frac{1}{2(z_{i+1/2} - z_{i-1/2})}\left(k_{s_{i-1/2}}\frac{T_{i-1}^{n+1} - T_i^{n+1}}{z_i - z_{i-1}} - k_{s_{i+1/2}}\frac{T_i^{n+1} - T_{i+1}^{n+1}}{z_{i+1} - z_i}\right)$$

$$+ \frac{1}{2(z_{i+1/2} - z_{i-1/2})}\left(k_{s_{i-1/2}}\frac{T_{i-1}^n - T_i^n}{z_i - z_{i-1}} - k_{s_{i+1/2}}\frac{T_i^n - T_{i+1}^n}{z_{i+1} - z_i}\right), \tag{24}$$

$$\frac{\eta_i^{n+1} - \eta_i^n}{\Delta t} = \frac{1}{z_{i+1/2} - z_{i-1/2}}\left(D_{\eta_{i-1/2}}\frac{\eta_{i-1}^{n+1} - \eta_i^{n+1}}{z_i - z_{i-1}} - D_{\eta_{i+1/2}}\frac{\eta_i^{n+1} - \eta_{i+1}^{n+1}}{z_{i+1} - z_i}\right)$$

$$+ \frac{1}{z_{i+1} - z_{i-1}}(K'_{\eta_{i+1}}\eta_{i+1}^{n+1} - K'_{\eta_{i-1}}\eta_{i-1}^{n+1}). \tag{25}$$

For the computation of soil moisture and temperature on the main levels, it is necessary to have midlevels at $i \pm 1/2$, where heat and moisture soil fluxes are calculated. The diffusional conductivity is evaluated at the middle of each soil layer from the soil moisture content on the main levels. At the bottom of the soil model, the values of temperature and moisture remain constant for the whole integration period. To close the system of equations for soil, the balance equations at the earth's surface must be solved.

The soil heat and moisture fluxes in the budget equa-

tions are determined directly from the gradients of temperature and moisture, respectively, between the ground surface and the first level in soil. However, there is no difference between CONTROL and SOIL in the calculation of radiation and latent and sensible atmospheric fluxes from the ground surface, and the explicit technique is used for their estimation.

The second modification, referred to as SOIL IMPLICIT, is an advanced variant of the first one, where the calculation of atmospheric surface fluxes in the heat and moisture balance equations is quite different. The

sensible and latent heat fluxes are computed from the gradients of temperature and mixing ratio, respectively, between the first level in the atmosphere and the ground surface and from the surface exchange coefficients determined with the help of the three-layer aerodynamic scheme (Pan et al. 1994). The values of temperature and mixing ratio are taken at the $(n + 1)$ time step. The finite-difference form of the heat balance equation (8) is then written as

$$\left(\frac{\Delta z_s \rho_s c_s}{\Delta t} + \frac{\Delta z_a c_p \rho_a}{\Delta t}\right)(T_g^{n+1} - T_g^n)$$

$$= \frac{K_t c_p \rho_a \pi_a}{z_a}(\Theta_a^{n+1} - \Theta_g^{n+1})$$

$$+ \frac{K_q \rho_a L_v}{z_a}(q_{v_a}^{n+1} - q_{v_g}^{n+1}) + \frac{\nu}{z_s}(T_g^{n+1} - T_s^{n+1}) + R_n^{n+1}, \tag{26}$$

where the net radiation at time step $n + 1$, R_n^{n+1}, is put in implicit form by approximating S^{n+1} by S^n and $T_g^{n+1^4}$ as $T_g^{n^3}(T_g^n + T_g^{n+1})/2$:

$$R_n^{n+1} = (1 - \alpha)S^n$$

$$- \epsilon_g\left[\sigma T_g^{n^3}\left(\frac{T_g^n + T_g^{n+1}}{2}\right) - F_L^n\right]. \tag{27}$$

For moisture, the balance equation (13) has the finite-difference form

$$\frac{\rho_w \Delta z_s}{\Delta t}(\eta_g^{n+1} - \eta_g^n)$$

$$= \frac{D_{\eta_g}}{z_s}(\eta_g^{n+1} - \eta_s^{n+1})\rho_w$$

$$- \frac{1}{2}(K'_{\eta_g}\eta_g^{n+1} + K'_{\eta_s}\eta_s^{n+1})\rho_w$$

$$+ \left[K_q\frac{(q_a - q_g)^{n+1}}{z_a} + I\right]\rho_a, \tag{28}$$

where $D_{\eta_g} = 1/2[D_\eta|_{z=0} + D_\eta|_{z=z_s}]$, $K'_{\eta_g} = K'_\eta|_{z=0}$, and $K'_{\eta_s} = K'_\eta|_{z=z_s}$.

Equations (26) and (28) are solved after the explicit calculation of Θ and q_v in the atmosphere. However, because of the implicit solution procedure, the values of the soil temperature and the volumetric soil moisture on the second soil level are not yet determined. A linear relation $(T_s^{n+1} = \beta T_g^{n+1} + \gamma)$ between the temperature at the first and second soil levels can be used to eliminate the unknown value of the soil temperature on the second soil level from (26) and to produce a linear equation for T_g^{n+1} and $q_{v_g}^{n+1}$ (Smirnova 1987; Pressman 1988). If there is saturation near the ground surface, that is, $q_{v_g} = q_{g_s}$, then T_g^{n+1} and $q_{g_s}^{n+1}$ can be related with sufficient accuracy using the Clausius–Clapeyron formula. If there is no saturation, (14) must be applied to eliminate q_{v_g}. In any

case, the heat balance equation (26) can then be solved to give the value of surface temperature T_g^{n+1} and corresponding $q_{v_g}^{n+1}$. This provides the mixing ratio $q_{v_g}^{n+1}$ from (14). If $q_{v_g}^{n+1} > q_{g_s}^{n+1}$, the excess defines the mixing ratio of the liquid phase, $q_{c_g}^{n+1}$, where $q_g^{n+1} = q_{v_g}^{n+1} + q_{c_g}^{n+1}$. The moisture balance equation (28) is then used to obtain the value of the soil moisture η_g at the interface with the atmosphere at the $(n + 1)$ time step.

The value of I used in (28) is obtained as follows when there is precipitation (zero otherwise). A maximum infiltration rate from the first to the second computational level in soil is calculated from (11) as the flux at the midpoint between the first and second computational levels in soil, assuming the saturation value of ground surface soil moisture. The actual value of I used in (28) is equal to the lesser of the precipitation rate and this maximum value. Surface runoff is then the difference (if positive) between the precipitation rate and the maximum infiltration rate. At this point, the upper boundary conditions for the soil domain have been determined and the temperature and the volumetric soil moisture may be finally calculated at each soil level.

The third modification of the model, referred to as PLANT, adds to the second version the effect of vegetation on surface processes. The finite-difference equivalents of (21) and (22) are expressed analogously to (26) and (28) and solved as in the second modification.

5. Results of the comparison

Since changes in the parameterization of ground surface interaction with the atmosphere strongly influence the forecast of ground surface values, diurnal changes of ground surface temperature will be compared. Our experiments are properly described as simulations rather than forecasts since the atmospheric properties are prescribed from observations rather than being predicted. In this way we can isolate errors in the model-produced ground surface temperature and fluxes as being caused by deficiencies in the soil model and surface energy budget.

a. Case study data

1) O'NEILL, NEBRASKA—8–9 AUGUST 1953: DRY CONDITIONS

The need for information necessary to initialize the soil model led to the use of data from the Great Plains Turbulence Field Program, conducted in O'Neill, Nebraska, 1 August–8 September 1953 (Lettau and Davidson 1957). In addition to detailed soil data, this experiment provided atmospheric data of sufficient time resolution to drive the soil model (appendix C), making this dataset well suited for this study.

A lee trough amplified over the northern High Plains during the first 12 h of the 24-h period used for inte-

gration of 1D models. This resulted in a low-level jet of over 20 m s^{-1} during the night of 8–9 August and strong surface winds from the south during the daytime hours of 9 August. The increase in moisture with this southerly flow resulted in some thin morning cloudiness on 9 August. Late in the integration period, clouds increased ahead of a cold front approaching from the northwest. There was no precipitation near the test site.

Initial values of volumetric soil water content are converted from gravimetric data published in Lettau and Davidson (1957, 398, Table 2.2.b) using a soil density of 1760 kg m^{-3}. For the CONTROL runs, the initial ground surface volumetric soil water content is derived from the measured value of soil moisture at 4-cm depth at 1300 CST 8 August from this table and equals 0.19 m^3 m^{-3}. The vertically averaged (deep soil) volumetric water content for the CONTROL is derived from the mean among table measurements at 10, 20, 40, and 80 cm and equals 0.09 m^3 m^{-3}. Soil temperatures are initialized using observations from Lettau and Davidson's Table 2.1.a (1957, 397). For the CONTROL model, T_m in (23) is assumed to be a deep soil temperature not affected by the diurnal cycle and is equal to 293.3 K. The thermal capacity of the slab per unit area, C_g, equals 98 790 J m^{-2} K^{-1}, calculated using the climatological value of thermal inertia for grassland in summer (Anthes et al. 1987).

Climatological values of emissivity (0.92; MM4 value) and roughness length (0.026 m; K. Mitchell 1995, private communication) are used.

The radiation fluxes are estimated at each time step for this experiment, and the existing dry and stable weather conditions allow us to minimize the errors connected with cloud in the calculation of incoming shortwave solar and longwave atmospheric radiation. The estimated absorbed solar radiation calculated in the model with climatological value of albedo for grassland equal to 0.19 is compared with the values of absorbed shortwave radiation derived from the observations of incoming solar radiation with the same value of albedo (Fig. 2). Both sets of observed shortwave radiation data, hourly averaged and 10-min averaged, are presented in this figure, together with the average between them. The discrepancies apparent on the figure from 1500 to 1900 UTC are attributable to a thin cloud layer noted over O'Neill during that time period, and the values estimated from the model lie between values derived from observations and close to the average of the two datasets. All other atmospheric characteristics, such as pressure, wind speed, potential temperature, and mixing ratio, are prescribed from the observations.

2) FIFE—1987: MOIST CONDITIONS

For the simulation of a moist situation, the FIFE [First ISLSCP (International Satellite Land Surface Climatology Project) Field Experiment] data are used. This experiment was conducted in grassland with gently roll-
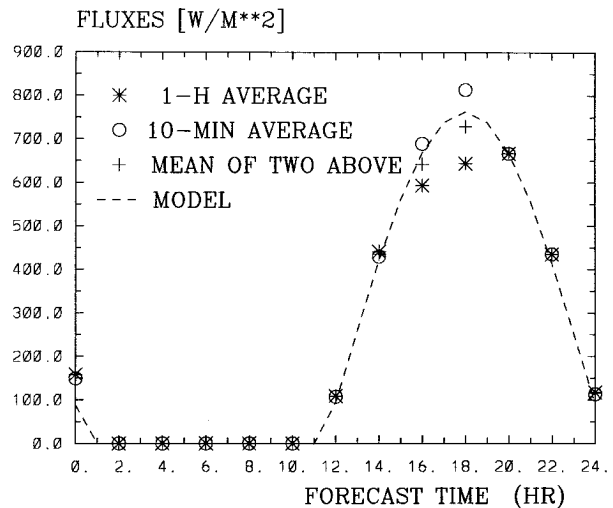

FIG. 2. Temporal variations of absorbed solar radiation, simulated and derived from hourly averaged and 10-min-averaged observations, and the mean between the two observed datasets for the O'Neill case (8–9 August 1953). Hour 0 is at 0035 UTC (1755 local solar time). This time convention is used for all time plots from the O'Neill case.

ing hills near Manhattan, Kansas, during 1987–89. The experiment site size was 15 km × 15 km, where the automatic meteorological stations and flux instrumentation were distributed. The available information about the soil and the ground surface was FIFE-site averaged and put together in FIFE-87 Compacted Surface Data Sets (CSDS) (Betts and Ball 1992). Soil moisture data is only available at 2.5 and 7.5 cm and is interpolated to initialize multilevel soil models. For the CONTROL runs, initial ground surface volumetric soil water content is derived from the 2.5-cm value and equals 0.39 m^3 m^{-3}, and the deep soil content is assumed to be the field capacity value equal to 0.34 m^3 m^{-3}. Initial soil temperatures were interpolated from the Betts and Ball data; the substrate value for the CONTROL runs, T_m, was the average at 50-cm depth for the simulation period. The thermal capacity of the slab per unit area, C_g, is 98 790 J m^{-2} K^{-1}, calculated using physical parameters for grassland in summer (Anthes et al. 1987). The same values of albedo and emissivity from O'Neill were used for FIFE, but with roughness length equal to 0.045 m (Chen et al. 1996).

Beside the information about the soil and the ground surface, time series data with 30-min frequency are also available for radiative fluxes, sensible and latent heat fluxes near the surface, atmospheric variables at one level near the ground surface, and also clouds and precipitation. For the purpose of the present study, a day with moist atmospheric conditions (with clouds and precipitation) and no data gaps (13 August) is chosen; the model initialization and the atmospheric forcing are provided by the CSDS, but the surface fluxes and the ground surface temperature are simulated and compared with those observed.
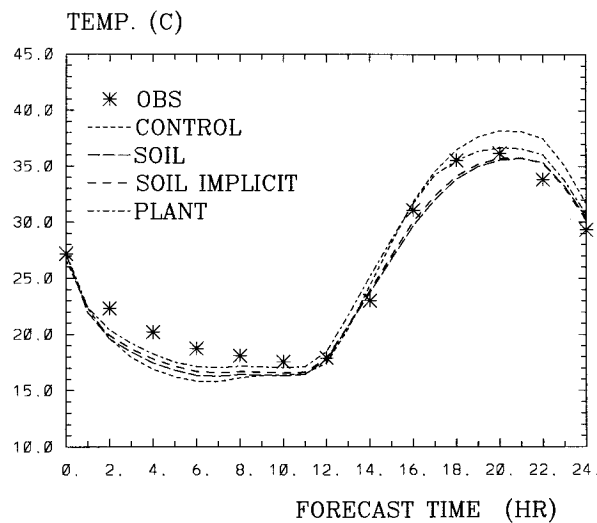
TEMP. (C)

FORECAST TIME (HR)

FIG. 3. Simulated diurnal variation of ground surface temperature by the basic model and its modifications (Table 1) as compared with observations at the depth of 0.5 cm for O'Neill case.

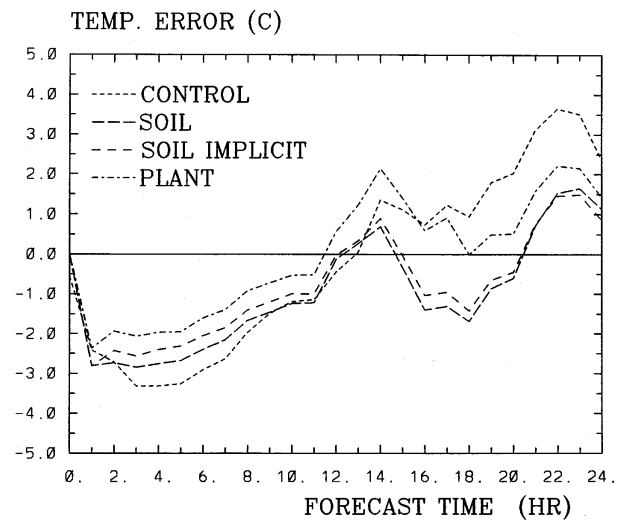TEMP. ERROR (C)

FORECAST TIME (HR)

FIG. 4. Diurnal variations of simulation errors (simulation minus observations) in ground surface temperature by the basic model and its modifications (Table 1) for O'Neill case.

b. Case study results

1) O'NEILL RESULTS

Figure 3 compares simulated and observed values of ground surface temperature for all four schemes described above (Table 1) for the O'Neill experiment. It can be seen that for the majority of the 24-h period, the PLANT modification gives the best forecast of ground surface temperature. For night hours the differences between schemes are small, although from 0235 UTC (1955 local solar time) up to 0935 UTC (0355 local solar time) both SOIL and SOIL IMPLICIT schemes are slightly better than the CONTROL. For daytime high temperatures, SOIL IMPLICIT and SOIL are only slightly cooler than the observed, while the CONTROL is too warm. The same conclusions are even more evident in Fig. 4, which shows the differences between the simulated and observed values. It should be noticed that all four error curves have two spikes: one in the early morning and another in the evening hours. There are two possible explanations for these error spikes. The first is the increase of the ground surface albedo at low solar angles, which is neglected in our experiments. The second is related to the presence of vertically oriented leaves in this grassland region; direct solar radiation will be largely precluded from reaching the ground surface early and late in the day because of interception and absorption by leaves of grass. Both effects could cause overestimation of the heating rate in the morning and underestimation of cooling near sunset.

It is important to note that the comparisons depicted in Figs. 3 and 4 are meaningful despite the fact that the observations are taken at 0.5 cm, whereas the simulated values are valid for a thin layer spanning the surface (Fig. 1). To be more accurate, we can compare the observed soil temperature at 0.5-cm depth with the sim-

ulated values at the same depth as long as they correspond to the first level in the soil model included in the SOIL, SOIL IMPLICIT, and PLANT schemes. Such comparisons have been conducted and showed that the range of simulated diurnal changes of temperature at 0.5-cm depth is slightly less than on the ground surface; that makes SOIL, SOIL IMPLICIT, and PLANT temperatures on the first soil level a little closer to the observations for most of the simulation period. Therefore, it appears safe to make conclusions based on the comparison of model ground surface temperatures with the observations at 0.5-cm depth.

It is also important to demonstrate that the variations between experiments are significant despite uncertainty in values of soil thermal conductivity or soil heat capacity. The soil properties for the described multilevel soil schemes are calculated at each time step according to (2), (3), (5), and (6), with the values of parameters taken from Cosby et al. (1984) for sandy loam. Since the O'Neill experiment provides actual observations of soil properties, the estimated magnitudes of the volumetric heat capacity averaged for the upper 10-cm layer and thermal conductivity averaged for the upper 5-cm layer can be compared to the corresponding observed values averaged for the same layers (Fig. 5). The measured heat capacity has significant time oscillations that are not described by (3), which depends only on the value of soil moisture. In this integration, the soil moisture decreases slightly in the upper layers from 0.18 m^3 m^{-3} at the beginning to 0.16 m^3 m^{-3} after 24 h. As a result, the calculated heat capacity remains almost constant for the whole forecast period, but its value is within the range of the O'Neill observations of this soil property. There is an even larger discrepancy between the estimated and observed thermal conductivity (Fig. 5), which occurs because of the difficulty in choosing prop-
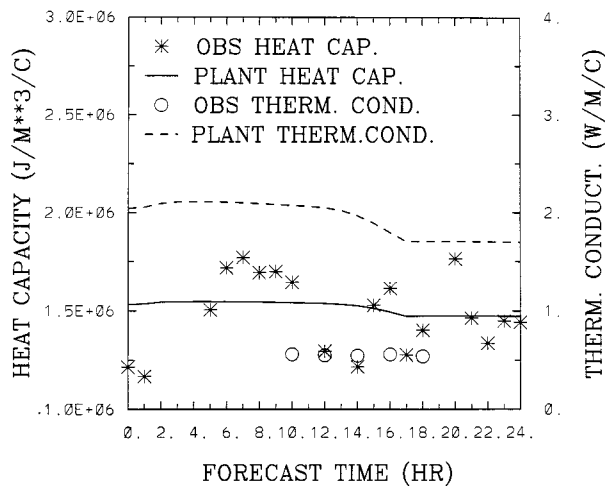
FIG. 5. Temporal variations of the observed and calculated (in PLANT) soil heat capacity averaged in the upper 10-cm layer and soil thermal conductivity averaged in the upper 5.5-cm layer for the O'Neill case.

er values of the parameters b and Ψ_s used in (2). Even for a given soil type, the standard deviation of these parameters could be up to 50% of the mean value (Cosby et al. 1984).

To investigate sensitivity to this uncertainty, integrations from four versions of the PLANT scheme are compared. The first version, called PLANT, is the basic model described in Table 1. In the second version, referred to as PLANT1, the calculated heat capacity in the top 10 cm of the soil is replaced by the observed values averaged for this layer. In the third version, called PLANT2, the observed thermal conductivity is used instead of the estimated value at the upper five levels, and

in the fourth scheme, referred to as PLANT3, both observed heat capacity and observed thermal conductivity are used.

Figure 6a reveals very little sensitivity of the temperature diurnal cycle to differences in volumetric heat capacity for the PLANT experiments, and the PLANT1 curve is very similar to that of PLANT. Use of the observed thermal conductivity, which is smaller than that obtained using (2) (recall Fig. 5), has more significant impact on the simulation of ground surface temperature (PLANT2 curve in Fig. 6a), increasing the range of temperature change from day to night in PLANT2 and PLANT3 relative to PLANT and PLANT1, and reducing the accuracy of temperature simulations, especially in the night hours.

Sensitivity to the assumed value of soil thermal capacity in CONTROL is also tested by replacing the climatological value by a different value based on observations (equal to 69 900 J m^{-2} K^{-1}, calculated with a constant value of $\nu = 1.32$ mcal cm^{-1} s^{-1} K^{-1} averaged over time and depth from Table 2.2.a of Lettau and Davidson, and $\rho_s c_s = 0.36$ cal cm^{-3} K^{-1} averaged from Table 2.2.c); this version of CONTROL is called CONTROL1. Since the value of soil thermal capacity derived from observations is smaller than the climatological value (CONTROL), it also produces an even larger temperature range and a poorer simulation (CONTROL versus CONTROL1 in Fig. 6b). Overall, the conclusions based on Figs. 3 and 4 are not changed by this experiment or by the experiment involving the different versions of PLANT described above. Furthermore, a fortuitous choice of parameters for the soil model cannot be responsible for the improvement of ground surface temperature forecast made by PLANT in comparison with the CONTROL scheme.
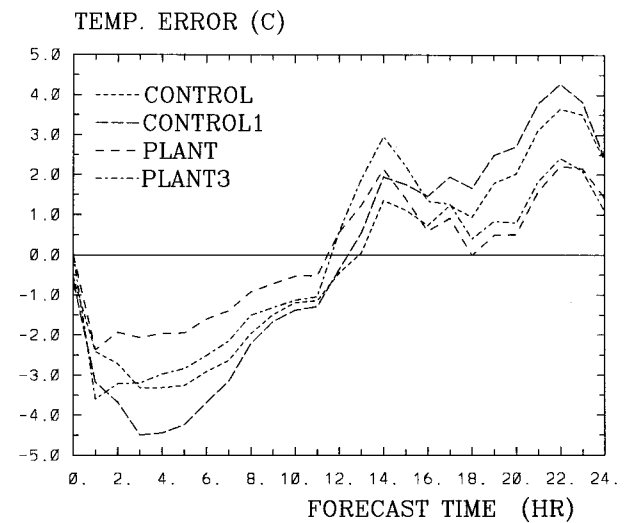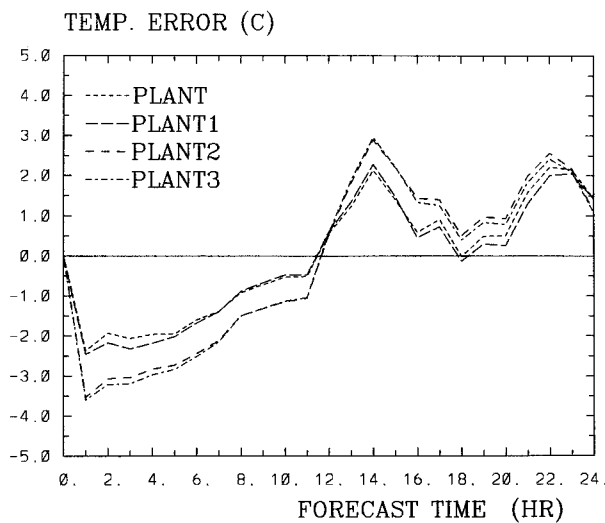

FIG. 6. Diurnal variations of simulation errors (simulation minus observations) in ground surface temperature by (a) PLANT and PLANT versions PLANT1 (with observed soil heat capacity), PLANT2 (with observed soil thermal conductivity), and PLANT3 (observed values for both soil heat capacity and thermal conductivity); (b) CONTROL and its version CONTROL1 (with observed value of thermal capacity), and PLANT and its version PLANT3 (observed values for both soil heat capacity and thermal conductivity) for O'Neill case.
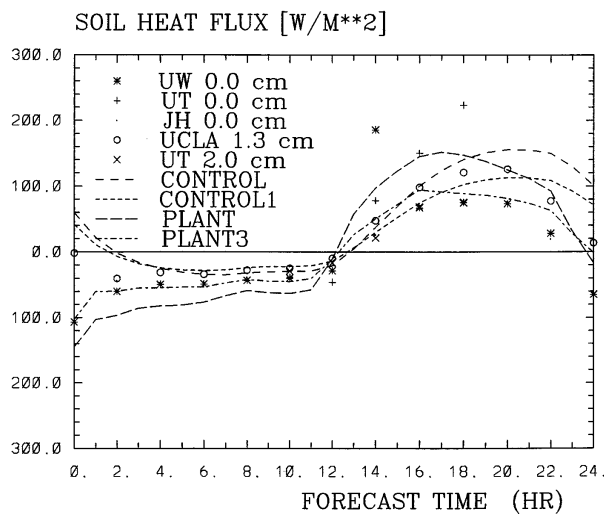
SOIL HEAT FLUX [W/M**2]

FIG. 7. Temporal variations of soil heat fluxes for O'Neill simulated by CONTROL, CONTROL1, PLANT, and PLANT3 models (Table 1) compared with observations on the ground surface by UW (University of Wisconsin), UT (University of Texas), and JH (Johns Hopkins University) at the depth of 1.3 cm by UCLA (University of California, Los Angeles) and at the depth of 2.0 cm by UT.

MOISTURE AVAILABILITY

FIG. 8. Temporal variations of ground surface moisture availability simulated using the four models (Table 1) for O'Neill case.

As a further check of sensitivity to assumed values of soil properties, for this same series of runs we compare temporal variations of simulated soil heat flux to observations. There are two factors complicating this comparison. First, there is a large scatter in soil fluxes measured by different investigators (Table 2.4 in Lettau and Davidson), especially during the daylight hours. Second is the significant change of soil flux with depth; the proper measurement depth for use in comparing with CONTROL is not precisely defined. However, Fig. 7 indicates that parameterization of soil processes by (23) in CONTROL and, particularly, CONTROL1, gives reasonable values of soil heat flux during most of the integration period. The positive values of soil heat flux for the first 2 h of integration in the CONTROL and CONTROL1 models mean that the ground surface is still transferring heat to the substrate layer, causing overestimation of the cooling rate during the evening and too cool temperatures at night. Values are in closer agreement with available observations during the night after the first 3 h. During the final 4 h of integration both CONTROL experiments also exhibit a substantial phase lag. The comparison of PLANT with PLANT3 also shows that observed values of soil properties improve the simulation of soil heat flux, especially in the night hours when there appeared to be more sensitivity of soil flux to the values of soil thermal conductivity and volumetric heat capacity.

Regarding the soil moisture evolution process (Fig. 8), the CONTROL model utilizing force restore treatment of ground soil moisture (Deardorff 1978) and calculating moisture availability as the ratio of simulated ground surface volumetric soil moisture to the field capacity value for O'Neill soil type dries out the observed
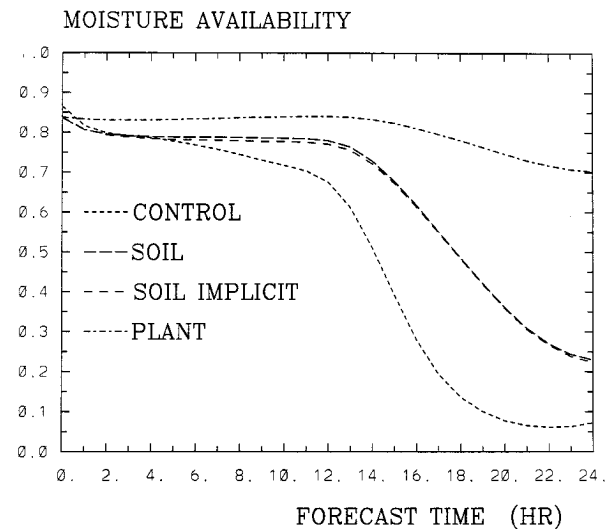
initial amount of soil moisture in the top layer more quickly than other three schemes. This causes the daytime temperatures in the CONTROL model to be considerably warmer than observed (Figs. 3 and 4) and may be connected with the semiempirical treatment of moisture transfer within soil and with the uncertainty in the determination of constants pointed out by Deardorff (1978). A similar decrease of soil moisture available for evaporation is also noted for the SOIL and SOIL IMPLICIT experiments (Fig. 8) where there is no vegetation and, therefore, no mechanisms preventing the overdrying of the soil. Only the addition of the evapotranspiration process (PLANT) makes the behavior of this variable more realistic. This result demonstrates the known importance of the vegetation cover in simulation of moisture exchange between the ground surface and the atmosphere.

The number of computational levels in soil necessary to accurately calculate soil contribution to the heat and moisture balance at the ground surface is also of interest. Therefore, simulations testing the sensitivity of ground surface temperature using the PLANT model to three different vertical resolutions were conducted. A three-level (0, 5 and 80 cm), five-level (0, 0.5, 5, 20, and 80 cm), and the standard nine-level configuration are compared with each other and with the CONTROL in Fig. 9. There is some discrepancy between the results for the five- and nine-level schemes, but they are close enough for this case to say that both schemes represent processes in the soil with fairly good accuracy. The simulations with the three-level soil scheme give quite different results. This occurs because the number of levels is not sufficient for satisfactory representation of heat and moisture transfer within the soil. Thus, it is preferable to have at least five levels in the soil model in this dry O'Neill case; on the other hand, the dryness clearly
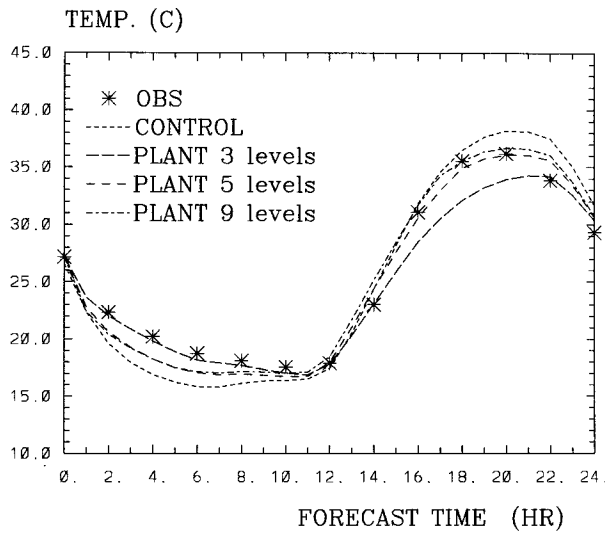
TEMP. (C)

FORECAST TIME (HR)

FIG. 9. As in Fig. 3 for three- and five-level versions of PLANT. The standard nine-level version of PLANT and the CONTROL curves from Fig. 3 are included for comparison.
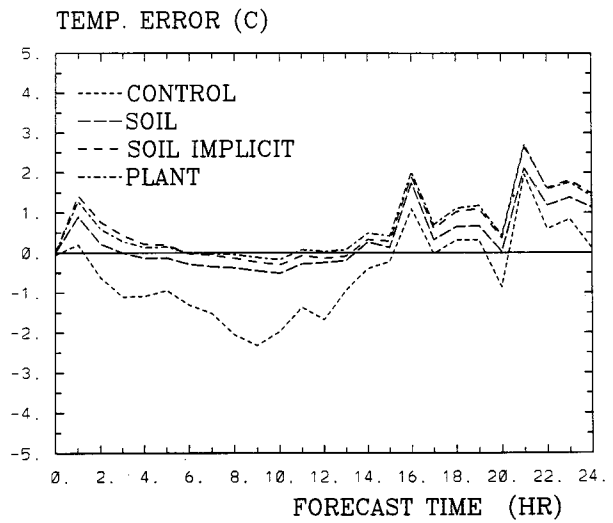
TEMP. ERROR (C)

FORECAST TIME (HR)

FIG. 10. As Fig. 4 for the FIFE case. Hour 0 is at 0015 UTC. This time convention is used for all time plots from the FIFE case.

increases sensitivity to vertical resolution, as will be seen by comparison with the moist FIFE case experiments described below.

2) FIFE RESULTS

The same experiments were also conducted for 13 August 1987, a moist day with clouds and precipitation chosen from the FIFE data. Figure 10 depicts the comparison of the ground surface temperature errors simulated by all four models described above. The advantage of the PLANT scheme in this case is not so evident, although there is a period at night between 5 and 13 h into the simulation when it is the most accurate among the schemes. However, all three soil model schemes give improvement over the excessively cool temperatures at night produced by CONTROL. As in the dry case, there is overestimation of the warming rate in the morning and underestimation of the cooling rate in the evening for all four schemes. The incoming solar radiation, substantially attenuated by cloud reflection and absorption for most of the day, has peaks in the morning and late afternoon hours. These periods also have higher values of standard deviations of incoming solar radiation, indicating partly cloudy skies over the experimental site. The degree of uncertainty in atmospheric forcing for these time periods may prevent better correspondence of simulated ground surface temperatures with the FIFE-site averaged values in these hours. The CONTROL scheme appears superior among all in the daytime hours (Fig. 10), but only because it is cooler than observations both at sunrise when warming starts and in the afternoon when cooling begins. Comparison of simulated soil heat fluxes with observations (Fig. 11) shows that differences are small between the models incorporating a soil

scheme. CONTROL is close to the observations during the daytime hours, but at night continues to be positive, indicating that the soil continues to transfer heat from the surface into the deeper layers. This may be the reason for excessive nighttime cooling, similar to that given by CONTROL in the O'Neill case. Tests with three versions of PLANT incorporating three-, five- and nine-level soil schemes show little sensitivity of ground surface temperature simulations to the vertical resolution of soil model for this moist day when soil moisture is close to saturation. However, the soil heat flux simulated with the three-level soil scheme is slightly less accurate than with the two other higher-resolution versions of PLANT.

SOIL HEAT FLUX [W/M**2]
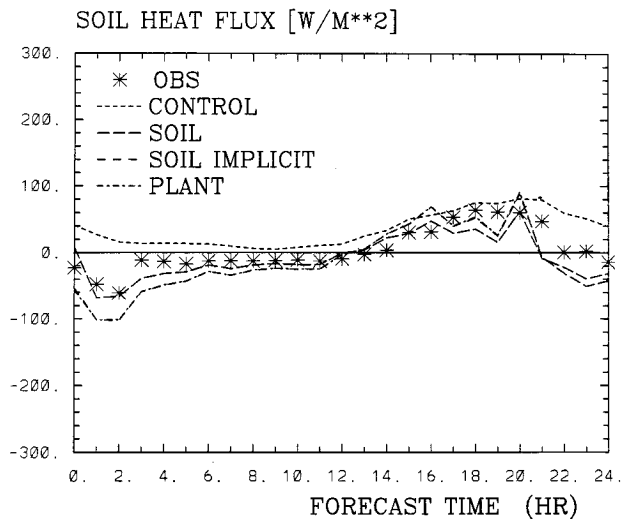

FORECAST TIME (HR)

FIG. 11. Temporal variations of soil heat fluxes simulated using four models (Table 1) for FIFE as compared with observations.

6. Discussion and conclusions

Three successive improvements to the treatment of the lower boundary for an atmospheric boundary layer model are described and then compared in tests against observations. These schemes are of increasing sophistication: adding a soil model, using an implicit solution procedure for calculating the surface fluxes, and using a simple vegetation model. Simulation tests of 24-h duration were made for these three schemes and a fourth (CONTROL) that incorporates a version of the force–restore treatment of ground surface temperature and soil moisture. These tests used data from a dry case (O'Neill) and a moist case (FIFE). Sensitivity tests were also made for the choice of soil parameters and vertical resolution. Predicted ground temperature and ground heat flux were compared among experiments and observations. The tests are summarized below.

In both the dry and moist cases, the ground temperature was underestimated at night by the CONTROL PBL model. Three modifications of the soil model, referred to above as SOIL, SOIL IMPLICIT, and PLANT, where the modeling of soil heat and moisture exchange processes and moisture balance equation is included, perform well at night in the moist case. In the dry case the soil model variations also underestimate night ground temperatures with only a slight improvement over the CONTROL results. Under O'Neill's dry soil conditions, the CONTROL PBL scheme is not very accurate in the daytime either. The incorporation of a simple soil model helps to solve this problem of excess daytime heating under dry conditions without degrading the surface temperature simulation under moist conditions.

As expected, the inclusion of parameterization of the evapotranspiration processes was very important when the soil moisture was close to the wilting point. In the O'Neill dry case, the evaporation process was affected by the reduced ability of plants to extract water, and the disregard of this effect causes excessive drying of soil and consequent errors in ground surface temperatures both in the CONTROL model and SOIL and SOIL IMPLICIT schemes. The experiments from the FIFE case show, alternatively, that when the soil moisture is near the saturation value, the addition of the vegetation model (PLANT) makes only small differences in simulations of ground temperature compared to soil models without vegetation (SOIL and SOIL IMPLICIT).

Overall, each configuration involving explicit computation of soil processes demonstrates some advantage over the original scheme for the computation of the surface fluxes in the heat and moisture balance equations. These configurations are more physically complete, and the difference in computation time between them and the CONTROL scheme is negligible. The sensitivity experiments with the PLANT scheme demonstrate that improvement over the CONTROL scheme is not simply achieved by fortuitous choice of values for soil parameters but is due to more accurate treatment of heat and moisture transports within soil, leading to a better description of the interaction processes between the ground surface and the atmosphere. The vertical resolution of the soil scheme incorporated into the PLANT model appeared to be much more important for the dry soil case when three levels are not sufficient for accuracy in the computation of soil heat and moisture fluxes near the surface.

Longer duration tests of this model using 5 months of FIFE data and other test cases developed for the PILPS (Project for Intercomparison of Land-surface Parameterization Schemes) have been conducted or are planned for the near future. Meanwhile, the results reported here and others reported elsewhere (Smirnova et al. 1996) have encouraged us to incorporate a five-level version of this model into a development version of MAPS with 40-km horizontal grid spacing. Results of the performance of the land-surface scheme in the context of this application will be reported at a later date.

APPENDIX A

List of Main Symbols

b	Empirical dimensionless factor dependent on soil type
c	Specific heat capacity of the layer spanning the ground surface
c_p	Specific heat of air under constant pressure
c_s	Specific heat capacity of soil
c_w	Specific heat capacity of water
C^*	Canopy water content (m)
C_g	The thermal capacity of the slab per unit area (J m^{-2} K^{-1})
D	Water drip rate from canopy to soil
D_η	Diffusional conductivity for soil (m^2 s^{-1})
E_c	The evaporation flux from the canopy
E_p, E	Potential and actual evaporation
E_{dir}	Evaporation flux from the bare soil
E_t	Transpiration flux
E_1	Surface flux of total moisture content
F_L	Incoming longwave radiation
G	Heat flux into the ground
$g(\eta_i)$	Dimensionless transpiration rate function
H	Sensible heat flux from ground
I	Infiltration flux
K_m	Heat transfer coefficient from ground to substrate in CONTROL

K_q — Turbulent exchange coefficient for moisture ($m^2 \, s^{-1}$)

k_s — Thermal diffusivity

K_t — Turbulent exchange coefficient for heat ($m^2 \, s^{-1}$)

k_v — Nondimensional plant resistance factor (=0.6)

K_η — Hydraulic conductivity in soil

K_{η_s} — Saturated soil value of hydraulic conductivity

K_η' — Linearized expression for hydraulic conductivity used in Eq. (25)

L_v — Latent heat of vaporization

M — Soil moisture availability

n — Dimensionless parameter (=0.5)

P — Precipitation flux

q_a — $= q_{v_a} + q_{c_a}$

q_g — $= q_{v_g} + q_{c_g}$

$q_{g_a}(T_g)$ — Saturation mixing ratio with respect to T_g

q_v — Atmospheric water vapor mixing ratio

q_{v_a}, q_{v_g} — Air mixing ratio at lowest model level and ground

q_{c_a}, q_{c_g} — Mixing ratio of liquid water in the air at lowest model level and ground

R_n — Net radiation

S — Incoming solar radiation

S' — Saturation water content for a canopy surface (=0.002 m)

T_g, T — Temperature at ground surface and in soil

T_m — Mean temperature of the substrate

T_s — Temperature at the second level in soil

W_s — Moisture flux into the ground

z — Vertical coordinate, increasing upward

z_a — Height at the lowest model level (10 m)

z_s — Depth of the first soil model level

Δz_a — $= 0.5 z_a$

Δz_i — Thickness of soil layer spanning soil level i [$= (z_i + z_{i-1})/2 - (z_i + z_{i+1})/2$]

Δz_s — $= -0.5 z_s$

α — Albedo of the ground surface

ϵ_g — Emissivity of the ground

η — Volumetric water content of soil (dimensionless)

η_g — Volumetric water content of soil at the ground surface

η_r — Residual volumetric water content in soil (=0.059 for sandy loam)

η_{ref} — Volumetric water content in soil (=0.25 for sandy loam), below which the transpiration rate begins to decrease due to a deficit of water

η_s — Porosity of soil

η_{wilt} — Volumetric water content in soil (=0.12 for sandy loam), below which the transpiration rate is zero

ν — Thermal conductivity of soil

Ω — Angular velocity of the earth (=7.2722 × $10^{-5} \, s^{-1}$)

π_a — Exner function at the lowest model level (10 m)

Ψ_s — Moisture potential for saturated soil

ρ — Density of the layer spanning the ground surface

ρ_a — Air density at the lowest model level

ρ_s — Soil density

ρ_ω — Water density

σ — Stefan–Boltzmann constant

σ_f — Nondimensional plant shading factor (=0.7)

Θ_a, Θ_g — Virtual potential temperature at lowest model level and ground

APPENDIX B

Definitions of Frequently Used Terms

A given volume V within the ground will contain water (either attached to soil particles or filling spaces between them), soil particles themselves, and air:

$$V = V_{water} + V_{soil} + V_{air}.$$

The quantity most frequently used to describe the amount of water in the soil is called soil volumetric water content, η. This quantity is defined as the ratio of water volume in the soil to the volume of moist soil, that is, for our hypothetical volume V,

$$\eta = \frac{V_{water}}{V}.$$

Figure B1 schematically illustrates certain important terms relating to the amount of water in the soil. (The precise values of η for each of these quantities is dependent on specific soil properties.)

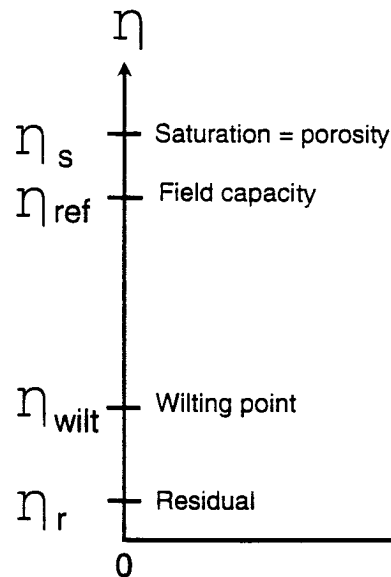These terms are defined as follows.

FIG. B1. Terms pertaining to soil volumetric moisture content.

- Residual, η_r: minimum realizable soil moisture content. Any remaining soil moisture is bound to soil particles and cannot escape to the atmosphere.
- Wilting point, η_{wilt}: minimum η for which plants are able to extract water from the soil.
- Field capacity, η_{ref}: the value of η above which there is no further increase in efficiency of extraction by plants of water from the soil.
- Saturation, η_s, also referred to as porosity: the state when all air in the soil has been displaced by water, that is, when V_{air} is zero. A volume is said to be saturated when it can accept no additional water.

APPENDIX C

Edited O'Neill Data

Data collected in the Great Plains Turbulence Field Program was compiled by Lettau and Davidson (1957). We used this data as the basis for prescribing atmospheric conditions above the surface in the one-dimensional calculations presented in section 5.

Rawinsonde observations were made at roughly 2-h intervals through the first general observation period of 8–9 August 1953. Careful inspection of this data as tabulated in Table 6.2 of Lettau and Davidson (1957, 403) revealed some obvious flaws, particularly in the temperature measurements. In order to construct a dataset suitable for our purposes, we found it necessary to subjectively quality control the rawinsonde observations by constructing a time–height series and subjectively analyzing for specific humidity and virtual potential temperature. In this analysis, we attempted to preserve the vertical structure revealed by the soundings, particularly the mixed layer and capping stable layer, while simultaneously smoothing in time where appropriate to remove temperature and humidity time fluctuations that appeared spurious. The analyzed fields were then reinterpolated to the original sounding data levels to constitute the quality-controlled dataset used in our simulations.

Inspection of the data suggested that the most reliable near-surface wind speed observations were the MIT (Massachusetts Institute of Technology) data at 2, 4, 8, and 16 m AGL (above ground level) tabulated in Table 4.1.b (Lettau and Davidson 1957, 401). The wind direction at these levels was assumed to be that measured at 16 m and tabulated in Table 1.2 (Lettau and Davidson 1957, 397). Single and double theodolite pibal observations were also taken, revealing in unusual temporal and vertical detail the winds at low levels. These data likewise were not of uniform quality. After eliminating tabulated observations that appeared clearly erroneous, the remaining wind information was subjectively combined and interpolated to height levels and rawinsonde observation times. For levels 50–500 m AGL, we used Tables 6.1b (Lettau and Davidson 1957, 403) and 6.3 (Lettau and Davidson 1957, 404), except where reliable

data were absent, in which case we used Table 6.2 (Lettau and Davidson 1957, 403). For levels above 500 m AGL, we used the rawinsonde observations of Table 6.2. Tables containing the quality-controlled temperature, mixing ratio, and wind profiles are available electronically by request to the corresponding author. It should be noted that only the time-interpolated near-surface values of these profiles were used as the atmospheric forcing for experiments described in this paper.

REFERENCES

Al Nakshabandi, G., and H. Kohnke, 1965: Thermal conductivity and diffusivity of soils as related to moisture tension and other physical properties. *Agric. Meteor.,* **2,** 271–279.

Anthes, R. A., 1984: Enhancement of convective precipitation by mesoscale variations in vegetative covering in semiarid regions. *J. Climate Appl. Meteor.,* **23,** 541–554.

——, E.-Y. Hsie, and Y.-H. Kuo, 1987: Description of the Penn State/NCAR Mesoscale Model Version 4 (MM4). NCAR Tech. Note NCAR/TN-282+STR, 66 pp. [Available from NCAR, P.O. Box 3000, Boulder, CO 80307-3000.]

Arakawa, A., 1972: Design of the UCLA general circulation model. Tech. Rep. 7, 103 pp. [Available from Dept. of Meteorology, c/o Mail Services, Box 951361, Los Angeles, CA 90095-1361.]

Avissar, R., and R. A. Pielke, 1989: A parameterization of heterogeneous land surfaces for atmospheric numerical models and its impact on regional meteorology. *Mon. Wea. Rev.,* **117,** 2113–2136.

Benjamin, S. G., K. A. Brewster, R. L. Brümmer, B. F. Jewett, T. W. Schlatter, T. L. Smith, and P. A. Stamus, 1991: An isentropic three-hourly data assimilation system using ACARS aircraft observations. *Mon. Wea. Rev.,* **119,** 888–906.

——, J. M. Brown, K. J. Brundage, D. Devenyi, B. E. Schwartz, T. G. Smirnova, T. L. Smith, and F.-J. Wang, 1996: The 40-km 40-level version of MAPS/RUC. Preprints, *11th Conf. on Numerical Weather Prediction,* Norfolk, VA, Amer. Meteor. Soc., 161–163.

——, J. M. Brown, K. J. Brundage, D. Devenyi, B. E. Schwartz, T. G. Smirnova, T. L. Smith, and A. Marroquin, 1997: Improvements in aviation forecasts from the 40-km RUC. Preprints, *Seventh Conf. on Aviation, Range, and Aerospace Meteorology,* Long Beach, CA, Amer. Meteor. Soc., 411–416.

Betts, A. K., and J. H. Ball, 1992: FIFE-1987 mean surface time series. Atmospheric Research. [Available from Alan Betts, Hendee Ln, Pittsford, VT 05763.]

Blackadar, A. K., 1976: Modeling the nocturnal boundary layer. Preprints, *Third Symp. on Atmospheric Turbulence, Diffusion, and Air Quality,* Raleigh, NC, Amer. Meteor. Soc., 46–49.

Bleck, R., and S. G. Benjamin, 1993: Regional weather prediction with a model combining terrain-following and isentropic coordinates. Part I: Model description. *Mon. Wea. Rev.,* **121,** 1770–1785.

Chen, F., K. Mitchell, J. Schaake, Y. Xue, H. Pan, V. Koren, Q. Duan, and A. Betts, 1996: Modeling of land-surface evaporation by four schemes and comparison with FIFE observations. *J. Geophys. Res.,* **101,** 7251–7268.

Clapp, R., and G. Hornberger, 1978: Empirical equations for some soil hydraulic properties. *Water Resour. Res.,* **14,** 601–604.

Cosby, B. J., G. M. Hornberger, R. B. Clapp, and T. R. Ginn, 1984: A statistical exploration of the relationships of soil moisture characteristics to the physical properties of soils. *Water Resour. Res.,* **20,** 682–690.

Deardorff, J. W., 1978: Efficient prediction of ground surface temperature and moisture with inclusion of a layer of vegetation. *J. Geophys. Res.,* **93,** 1889–1903.

de Vries, D. A., 1952: The thermal conductivity of granular material. *Bull. Inst. Intern. Froid,* 115–131.

——, 1958: A simultaneous transfer of heat and moisture in porous media. *Trans. Amer. Geophys. Union,* **39**(5), 909–916.

Dickinson, R. E., 1984: Modeling evapotranspiration for three-dimensional global climate models. *Climate Processes and Climate Sensitivity, Geophys. Monogr.,* No. 29, Amer. Geophys. Union, 58–72.

——, A. Henderson-Sellers, P. J. Kennedy, and M. F. Wilson, 1986: Biosphere–atmosphere transfer scheme (BATS) for the NCAR Community Climate Model. NCAR Tech. Note NCAR/TN-275 + STR, 69 pp. [Available from NCAR, P.O. Box 3000, Boulder, CO 80307.]

Estoque, M. A., and J. M. Gross, 1981: Further studies of a lake breeze. Part II: Theoretical study. *Mon. Wea. Rev.,* **109,** 619–634.

Garrett, A. J., 1982: A parameter study of interactions between convective clouds, the convective boundary-layer, and forested surface. *Mon. Wea. Rev.,* **110,** 1041–1059.

Grell, G. A., J. Dudhia, and D. R. Stauffer, 1994: A description of the fifth-generation Penn State/NCAR Mesoscale Model (MM5). NCAR Tech. Note NCAR/TN-398 + STR, 138 pp. [Available from NCAR, P.O. Box 3000, Boulder, CO 80307.]

Halstead, M. H., R. L. Richman, W. Covey, and J. D. Merryman, 1957: A preliminary report on the design of a computer for micrometeorology. *J. Meteor.,* **14,** 308–325.

Jacobsen, I., and E. Heise, 1982: A new economic method for the computation of the surface temperature in numerical models. *Contrib. Atmos. Phys.,* **55,** 128–142.

Kiselnikova, V. Z., E. M. Pekelis, D. Ya. Pressman, N. F. Veltischev, and A. A. Zhelnin, 1984: Application of mesoscale numerical model to local weather prediction. *Proc. Nowcasting-II Symp.,* Nörrkoping, Sweden, European Space Agency, 301–307.

Lettau, H. H., and B. Davidson, 1957: *Exploring the Atmosphere's First Mile.* Vol. I. Pergamon Press, 376 pp.

——, and ——, 1957: *Exploring the Atmosphere's First Mile.* Vol 2. Pergamon Press, 202 pp.

Mahrer, Y., and R. A. Pielke, 1977: A numerical study of the air flow over irregular terrain. *Contrib. Atmos. Phys.,* **50,** 98–113.

Mahrt, L., and H.-L. Pan, 1984: A two-layer model of soil hydrology. *Bound.-Layer Meteor.,* **29,** 1–20.

Manabe, S., D. G. Hahn, and J. L. Holloway Jr., 1974: The seasonal variation of the tropical circulation as simulated by a global model of the atmosphere. *J. Atmos. Sci.,* **31,** 43–83.

Matthews, E., 1984a: Prescription of land-surface boundary conditions in GISS GCMII. NASA Tech. Memo 86096, 20 pp. [Available from NASA, Goddard Institute for Space Studies, 2880 Broadway, New York, NY 10025.]

——, 1984b: Vegetation, land-use and seasonal albedo data sets: Documentation of archived data tape. NASA Tech. Memo. 86107, 9 pp. [Available from Goddard Institute for Space Studies, 2880 Broadway, New York, NY 10025.]

McCumber, M. C., 1980: A numerical simulation of the influence of heat and moisture fluxes upon mesoscale circulations. Ph.D. dissertation, University of Virginia, 255 pp. [Available from University Microfilms International, P.O. Box 1346, Ann Arbor, MI 48106-1346.]

——, and R. A. Pielke, 1981: Simulation of the effects of surface fluxes of heat and moisture in a mesoscale numerical model. *J. Geophys. Res.,* **86,** 9929–9938.

Pan, H.-L., and L. Mahrt, 1987: Interaction between soil hydrology and boundary-layer development. *Bound.-Layer Meteor.,* **38,** 185–202.

Pan, Z., S. G. Benjamin, J. M. Brown, and T. Smirnova, 1994: Comparative experiments with MAPS on different parameterization schemes for surface moisture flux and boundary-layer processes. *Mon. Wea. Rev.,* **122,** 449–470.

Philip, J. R., and D. A. de Vries, 1957: Moisture movement in porous materials under temperature gradients. *Trans. Amer. Geophys. Union,* **38,** 222–232.

Physick, W., 1976: A numerical model of the sea-breeze phenomenon over a lake or gulf. *J. Atmos. Sci.,* **33,** 2107–2135.

Pielke, R. A., 1974: A three-dimensional numerical model of the sea breeze over south Florida. *Mon. Wea. Rev.,* **102,** 115–139.

Pressman, D. Y., 1988: Postanovka i algoritm chislennogo resheniya zadachi lokalnogo prognoza (An algorithm of numerical solution for local weather forecasting system). *Trudy GMTs SSSR,* **298,** 11–23.

Richards, L. A., 1931: Capillary conduction of liquids through porous mediums. *Physics,* **1,** 318–333.

Sellers, P. J., Y. Mintz, Y. C. Sud, and A. Dalcher, 1986: A simple biosphere model (SiB) for use within general circulation models. *J. Atmos. Sci.,* **43,** 505–531.

Sievers, U., R. Forkel, and W. Zdunkowski, 1982: Transport equations for heat and moisture in the soil and their application to boundary layer problems. *Beitr. Phys. Atmos.,* **56,** 58–83.

Smirnova, T. G., 1987: Ob ispolzovanii uravnenyi balansa tepla i vlagi v zadache lokalnogo prognoza pogody (Use of heat and moisture balance equations in local weather prediction). *Meteor. Gidrol.,* **6,** 15–22.

——, J. M. Brown, and S. G. Benjamin, 1996: The soil component of the MAPS model: Description and performance in one- and three-dimensional applications. Preprints, *11th Conf. on Numerical Weather Prediction,* Norfolk, VA, Amer. Meteor. Soc., 259–261.

Smith, C. B., M. N. Lakhtakia, W. J. Capehart, and T. N. Carlson, 1994: Initialization of soil-water content for regional-scale atmospheric prediction models. *Bull. Amer. Meteor. Soc.,* **75,** 585–593.

Tremback, C. J., and R. Kessler, 1985: A surface temperature and moisture parameterization for use in mesoscale numerical models. Preprints, *Seventh Conf. on Numerical Weather Prediction,* Montreal, PQ, Canada, Amer. Meteor. Soc., 355–358.

Wetzel, P. J., 1978: A detailed parameterization of the atmospheric boundary layer. Ph.D. dissertation, Colorado State University, 195 pp. [Available from Dept. of Atmospheric Science, Colorado State University, Fort Collins, CO 80523.]

——, and J.-T. Chang, 1988: Evapotranspiration from nonuniform surfaces: A first approach for short-term numerical weather prediction. *Mon. Wea. Rev.,* **116,** 600–621.

Wilson, M. F., A. Henderson-Sellers, R. E. Dickinson, and P. J. Kennedy, 1987: Sensitivity of the Biosphere–Atmosphere Transfer Scheme (BATS) to the inclusion of variable soil characteristics. *J. Climate Appl. Meteor.,* **26,** 341–362.

Zhang, D.-L., and R. A. Anthes, 1982: A high-resolution model of the planetary boundary layer–sensitivity tests and comparisons with SESAME-79 data. *J. Appl. Meteor.,* **21,** 1594–1609.

Zobler, L., 1988: A world soil file for global climate modeling. NASA Tech. Memo. 87802. [Available from NASA Goddard Institute for Space Studies, 2880 Broadway, New York, NY 10025.]